Proceedings of ASME Turbo Expo 2011
GT2011
June 6-10, 2011, Vancouver, British Columbia, Canada

GT2011-45916

ANALYSIS OF FLOW MIGRATION IN AN ULTRA-COMPACT COMBUSTOR

Brian T. Bohan and Marc D. Polanka
Air Force Institute of Technology
WPAFB, OH 45433

ABSTRACT

The Ultra Compact Combustor (UCC) has the potential to offer improved thrust-to-weight and overall efficiency in a turbojet engine. The thrust-to-weight improvement is due to a reduction in engine weight by shortening the combustor section through the use of the revolutionary UCC design. The improved efficiency is achieved by using an increased fuel-to-air mass ratio, and allowing the fuel to fully combust prior to exiting the UCC system. Furthermore, g-loaded combustion offers increased flame speeds that can lead to smaller combustion volumes. The circumferential combustion of the fuel in the UCC cavity results in hot gases present at the outside diameter of the core flow. This orientation creates an issue in that the flow from the circumferential cavity needs to migrate radially and blend with the core flow to present a uniform temperature distribution to the high-pressure turbine rotor. A computational fluid dynamics (CFD) analysis is presented for the flow patterns in the combustor section of a representative fighter-scale engine. The analysis included a study of secondary flows, cavity flow characteristics, shear layer interactions and mixing properties. An initial understanding of primary factors that impact the radial migration is presented. Computational comparisons were also made between an engine realistic condition and an ambient pressure rig environment.

NOMENCLATURE

b	Vane Chord
CFD	Computational fluid dynamics
EGV	Exit Guide Vane
g	Gravity
g_c	Newtons constant
ID	Inside diameter
IGV	Inlet guide vane
LBO	Lean blow out
OD	Outside diameter
PF	Pattern factor
RANS	Reynolds Averaged Navier-Stokes
r_{cav}	Cavity Radius
Re	Reynolds Number
S_B	Bubble Velocity
s	Second, spacing
T_t	Total temperature
Tu	Turbulence intensity
UCC	Ultra-compact combustor
V_{tan}	Tangential Velocity
Z	Zweifel load coefficient
β_1	Vane inlet angle
β_2	Vane exit angle

INTRODUCTION

A large majority of the current axial turbine engines in operation today utilize a combustor design that in principle has not changed since the creation of the jet engine in 1929. The materials in the combustor have been updated to handle higher temperatures and with the introduction of film cooling, the combustion temperatures can exceed the material failure temperature of the combustor liner. The concept of the traditional combustor uses axial flow straightened by the compressor exit guide vane (EGV) and a long combustion region on the order of 25-50 centimeters to fully combust the fuel prior to entering the high-pressure turbine inlet guide vane (IGV). Historically, turbine engine combustion has taken place at an overall fuel-to-air ratio much

less than stoichiometric [1]. Combining the low fuel-to-air ratio and the long combustor sections allowed the fuel and air to mix, evaporate, and fully burn prior to exiting the combustor section. To improve engine efficiency and specific thrust the value of the turbine inlet temperature (T_{t4}) has been steadily increased. Increased combustion temperatures can be achieved by increasing the fuel-to-air ratio closer to stoichiometric. In recent years, the effort to improve the thrust-to-weight ratio of turbine engines has led to advanced combustors which are more compact than the traditional combustor discussed above [2]. Combining the effects of decreased combustor volume with an increased fuel-to-air ratio increases the possibility of unburned fuel entering the turbine section. An ultra-compact combustor is a potential solution to an increase in T_{t4} and a decrease of up to 66% [3] in the length of the combustor section which could lead to improved efficiency and an increased specific thrust. The UCC features a circumferential cavity positioned around the outside diameter (OD) of the engine as shown in the upper part of Figure 1. The lower portion of Figure 1 contrasts the orientation of components in an ultra-compact combustor with a traditional combustor highlighting the axial length differences.

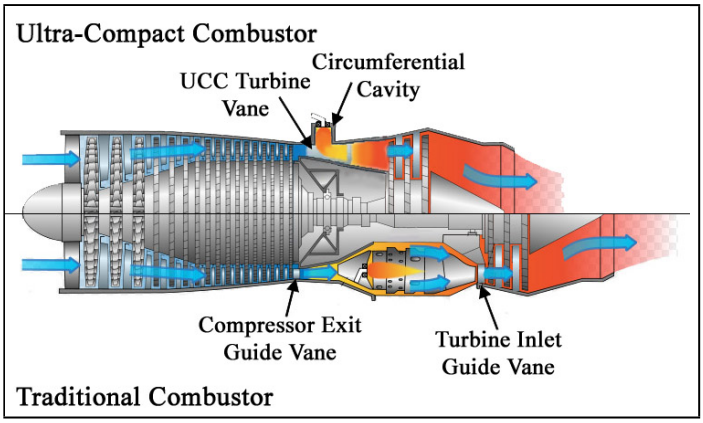

FIGURE 1: UCC and traditional combustor systems comparison

Within the UCC, the compressor exit guide vane and the turbine IGV are combined into a single airfoil located directly below the UCC cavity. Fuel and air are injected into the cavity at an angle to allow the fuel and air to mix and swirl in the circumferential direction around the OD. This circumferential versus axial burning increases the g-loading on the fluid and provides two benefits. The first benefit is that combustion products burned under increased g-loading experience increased flame speeds as introduced by Lewis [4] in 1973. The second benefit is that the heavier, unburned fuel particles are forced to the outside diameter of the circumferential cavity by the g-force. This migration ensures that these particles stay in the cavity until they are consumed and converted to lighter exhaust products. The lighter exhaust products are pushed toward the inside diameter of the circumferential cavity where they exit the cavity and interact with the turbine vanes. Allowing the heavy unburned fuel to remain in the circumferential cavity until it is fully broken down is the equivalent of an infinite combustion section which only occupies about 5 cm of axial length.

The research presented in this paper analyzed the impact of turbine vane spacing, air inlet port sizing, and UCC inlet mass flow variations on the velocity and swirling mass flow rate of the fluid in the circumferential cavity and the resulting temperature profile at the exit to the UCC section.

THEORY & PREVIOUS RESEARCH

The UCC initially conceived by Sirignano [5] takes advantage of circumferential combustion versus axial combustion supplemented with an additional benefit of an increased flame speed resulting from g-loaded combustion. This finding was originally documented by Lewis [4] who reported that beginning at 200 g's the flame speed began to increase. From 500 to 3,500 g's there was a steady increase in flame speed with increasing centrifugal force. In this range, Lewis found that the burning rate of the fuel-air mixture was proportional to the square root of the g-loading. Lewis attributed the increase in flame speed to the presence of bubbles or eddies that traveled ahead of the flame front due to the centripetal acceleration. When the bubble velocity (S_B) exceeds the turbulent flame speed, the flame propagates at the bubble velocity given by Eq. 1 [4]:

$$S_B = 1.25\sqrt{g}, \tag{1}$$

where g is the g-loading. The units for Eq. 1 are ft/s. Lewis noted that 1.25 coincidently is the 1g bubble velocity in ft/s. The g-loading value as defined by Zelina et al. [3] is given in Eq. 2.

$$g = \frac{V_{tan}^2}{g_c r_{cav}}, \tag{2}$$

In Eq. 2, V_{tan} is the tangential velocity in the cavity (m/s), g_c is Newtons constant (m/s^2) and r_{cav} is the average cavity radius (m). Below 200 g's Lewis showed that the turbulent flame speed controls the flame propagation and the velocity is independent of g-loading. Above 3,500 g's Lewis noted a sharp decrease in flame speed until a combustion limit was reached and blowout occurred.

Initial experimental studies by Zelina et al. [2] on small scale UCC systems operating at atmospheric and increased pressures showed a combustion efficiency between 95 and 99% over a wide range of operating conditions burning JP-8 +100 fuel. Additionally, this study noted that the axial flame length from the UCC was approximately 50% shorter than conventional combustion systems. The results from a series of lean blowout (LBO) tests conducted by Zelina et al. [2] which recorded the equivalence ratio in the cavity at blowout for varying g-loading is shown in Figure 2. Zelina et al. found that a stable flame could be maintained over a wide range of operating conditions with a maximum g-loading value approximated between 7,000 and 8,000 g's. This maximum g-loading value is supported by the data presented by Lewis [4].

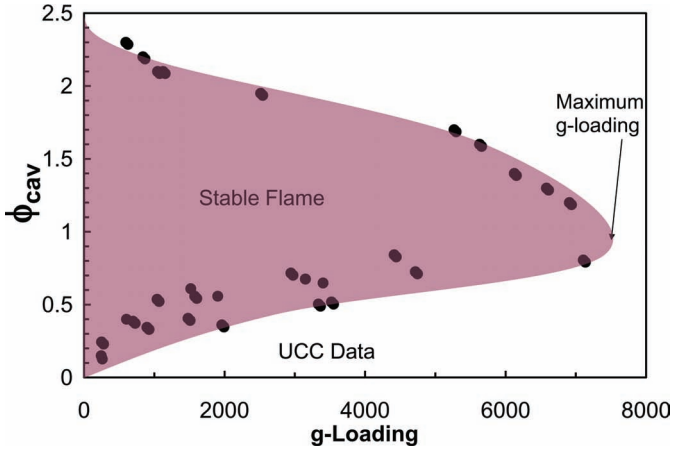

FIGURE 2: UCC Cavity Equivalence Ratio at Blowout as a Function of Cavity g-Loading [2]

The UCC turbine vanes experience fluid interactions from two directions, one of which is a cross flow. When a body with an endwall exists in cross flow, the effects of secondary flows must be considered. Langston [6] provided much of the early work regarding secondary flows and identified the dominant vortical structures that form around a body protruding from a surface known as a horseshoe and passage vortex. In a turbine engine, the vortex structures can make film cooling difficult by disrupting the expected flow pattern of the cooling film in addition to increasing the convective heat transfer and producing aerodynamic losses. Much of the research regarding secondary flows has been in the turbine region of an engine that uses a conventional combustion system. The long can-type combustor provides an undisrupted surface where a thick boundary layer could form. Hermanson and Thole [7] [8] studied the effect of inlet conditions and Mach number on the formation of secondary flows. The inlet in their study was the exit condition of the combustor section. Their research showed that thicker boundary layers resulted in a horseshoe vortex that spread further around the leading edge. Additionally, they showed that when no stagnation pressure gradient was present, no horseshoe or passage vortex formed.

In the current study, several factors that impact the temperature profile at the exit to the UCC section were studied. One area was the secondary flow along the OD endwall of the vane as it encountered the shear from the cavity circumferential flow. This interaction could be exploited in aiding the migration of the hot flow exiting the cavity. The migration across taller vanes than previously experimented with is one of the key aspects of the current study. Understanding the flow properties across taller vanes will be an important factor as the UCC transitions from small scale testing to a larger fighter-scale. To the knowledge of the authors no research has been performed on a UCC for a fighter-scale engine.

UCC GEOMETRY

A traditional combustor section of a fighter-scale engine features a compressor exit guide vane to turn the flow axial prior to entering the combustor, and a turbine inlet guide vane at the exit of the combustor to provide fluid at the correct angle to the first turbine stage. In a UCC, the compressor EGV and the turbine IGV are combined into a single vane located directly below the UCC cavity. Figure 3 shows the orientation and dimension of components in the ultra-compact combustor tested in this study. The combustor section inlet is on the left of Figure 3 with the combustion products exiting to the right. The inlet and exit dimensions were sized to nominal fighter-scale engine dimensions for the compressor exit and the turbine inlet passages, respectively. The inner radius of the passage at the exit was 31.75 centimeters with an outer radius of 38.1 centimeters. The passage expansion was performed at a shallow 7° angle per wall to prevent separation in the adverse pressure gradient region. Temperature profiles discussed later are taken at the inlet to the turbine rotor labeled 'Temperature Plane'.

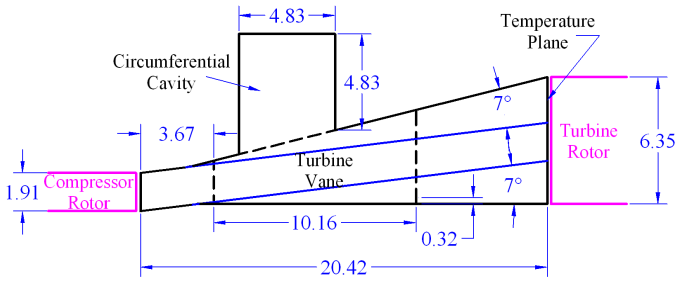

FIGURE 3: Cross-sectional view of UCC section used in the current analysis (Dimensions are in centimeters)

For the current study a new UCC turbine vane was developed which was a composite of a representative compressor EGV and turbine IGV. With the compressor EGV removed, this "hybrid" vane allowed the fluid exiting the compressor to maintain its swirl as it entered the UCC section. The fluid was then turned slightly to achieve an exit angle of 70° into the high-pressure turbine. The hybrid vane only required 16° of turning and had a Zweifel load coefficient of 0.70. The Zweifel load coefficient was calculated using the definition presented by Baskharone [9] shown in Eq. 3.

$$Z = 2\frac{b}{s}cos^2\beta_2(tan\beta_1 - tan\beta_2) \quad (3)$$

In Eq. 3, s is the vane spacing, b is the vane chord, β_1 is the vane inlet angle and β_2 is the vane exit angle. Figure 4 shows the development of the hybrid vane shape and its relative positioning to the UCC circumferential cavity. The axial chord of this vane was also set at 10.16 centimeters, however, due to the steep angle of the vane, the chord length was 21.07 centimeters. The maximum vane thickness was 2.07 centimeters to enable later internal cooling passages in the airfoil. Due to the orientation and thickness of the hybrid vane, metallic blockage of the core flow and overlap occurred if the number of vanes was increased beyond 30. The leading edge of the vane was positioned upstream of the circumferential cavity to introduce the hot gases from the cavity prior to the throat of the vane passage to aid in mixing with the core flow. The cavity was positioned upstream in the passage to allow fluid exiting the cavity to more easily span a shorter radial distance and provide a more uniform temperature distribution downstream. Additionally, positioning the cavity upstream in the passage provided the greatest length for mixing of the core flow with the hot cavity flow.

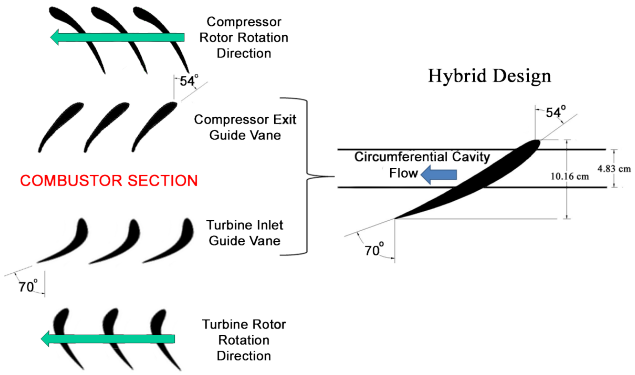

FIGURE 4: Origin and orientation of the hybrid vane design

NUMERICAL SETUP

A numerical analysis was used to characterize the flow conditions in the UCC test section over a wide range of flow and geometry variations. This analysis provided the preliminary research on fighter-scale UCC performance. All solutions were run using FLUENT® 6.3 with a 3-dimensional, node centered, steady-state, pressure-based solver with a RANS turbulence model. The SIMPLE algorithm was selected for pressure-velocity coupling which uses a relationship which enforces mass conservation and establishes the pressure field within the domain. All solutions were run second-order for momentum, density and energy. Turbulent production and dissipation along with pressure were kept first-order to aid computational speed and stability. The surface meshes in the computational domain were resolved with a combination of structured and unstructured cells. Structured cells defined the surface of the vane while unstructured cells were used on the remaining surfaces in the geometry. A single unstructured block resolved the domain volume. All mesh generation was performed in Gridgen® and exported for use in FLUENT®.

Following the findings of Hermanson and Thole [8], the $k-\epsilon$ RNG turbulence model was selected for the current analysis for the models' ability to handle stagnation flows and conditions with high streamline curvature. Hermanson and Thole were able to compare experimental results to various numerical simulations using different turbulence models and found that the $k-\epsilon$ RNG turbulence model most closely matched the experimental flow pattern and vorticity magnitude.

A small secondary flow study was conducted using a simplified UCC geometry to verify that the $k-\epsilon$ RNG turbulence model would produce a horseshoe and passage vortex using the grid and solver settings described above. This study concluded that the $k-\epsilon$ RNG turbulence model combined with the tested grid resolution were capable of generating the appropriate secondary flows.

UCC COMPUTATIONAL DOMAIN

The UCC computational domain consisted of a single vane extracted from the complete three-dimensional UCC section. Figure 5a shows the domain highlighted from the full annulus and Figure 5b shows the periodic test domain with boundary conditions. All non-labeled boundaries were walls. Domain sections were created for the hybrid vane featuring 20 vanes and 30 vanes arrayed around the complete UCC annulus. As the number of turbine vanes arrayed around the complete annulus was increased, the width of the computational domain was decreased to maintain only one vane in the domain. Table 1 summarizes the specifica-

tions of the vane and domain sections. In addition to the baseline UCC air injector ports which had a diameter of 0.54 centimeters, additional domains were created for the 20- and 30-vane test cases which increased the diameter of the air injector ports to approximately 2 times and 3 times the baseline diameter. The 30-vane domain could not fit the 3x diameter inlet ports without overlapping so this condition was not tested in that domain. The inlet variation was used to test the impact of the injection velocity on the flow properties, specifically the tangential velocity, in the circumferential cavity. Figure 6 shows the three air inlet port variations. A final increase in inlet area was created by converting the upper wall of the baseline geometry circumferential cavity to a mass flow inlet and the inlet ports were converted to walls. Since all inlet port holes were drilled at an angle relative to the tangent of the circumferential cavity, the inlet and exit of the air inlet ports were elliptic and thus were larger than the cross-sectional area of the hole. Table 2 shows the port diameter and total inlet area for each domain section of the 20- and 30-vane variants. While the diameter of the ports was increased, the on-center spacing for all configurations was held constant. All ports injected air into the cavity at 35° relative to the tangent of the cavity. In the 20-vane domain, a total of 80 pairs of air injector ports were used, this resulted in 8 ports per domain section. The number of ports in the 30-vane domain was set to 90 pairs of ports around the complete UCC section to maintain as close to 80 pairs as possible without having partial holes in individual domains sections. The hole spacing and total number of ports for each domain tested are also shown in Table 1.

TABLE 1: UCC turbine vane spacing and circumferential cavity inlet port specifications per section

Parameter	20-Vane	30-Vane
Vane Spacing (cm)	10.0	6.65
Throat Width (cm)	2.82	1.34
Axial Solidity	2.09	3.11
Number of Air Inlet Ports	8	6
Air Inlet Port Spacing†(cm)	3.16	2.81
Air Inlet Port Spacing (deg)	4.5	4

† Linear distance between hole centers

A grid independence check was performed to ensure the resolution of the computational domain was not influencing the test results, specifically the tangential velocity in the circumferential cavity. The variation of tangential velocity with increasing grid resolution from 1.5 to 4.3 million cells was found to be less than 2.4% across all resolutions. A variation of less than 5% within the CFD solution is considered independent and thus all resolutions could have been used.

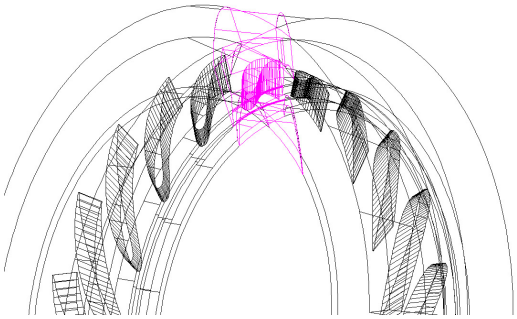

(a) Domain relative to full array

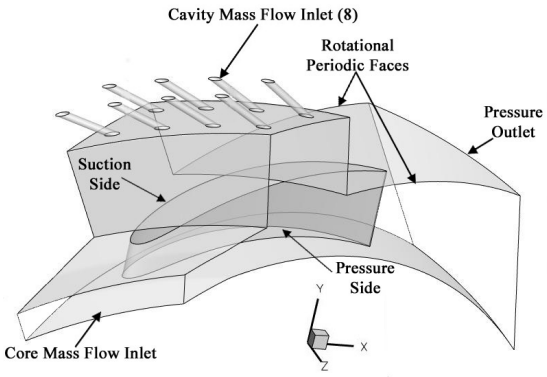

(b) Periodic Domain

FIGURE 5: 20-vane (hybrid vane style) computational domain

The computation time for each cell resolution was acceptable so the largest cell volume was selected for each domain to ensure sufficient resolution of the secondary flows.

COMPUTATIONAL TEST CONDITIONS

For ground takeoff, the total fuel burn for the fighter-scale engine was approximated at 2 kg/s. The compressor was estimated to provide air at a total flow rate of 72 kg/s. Removing flow for turbine cooling left 66 kg/s usable mass flow. Based on previous work, the remaining core flow was split such that the mass flow rate into the circumferential cavity was approximately 30% that of the core flow rate. The resulting core mass flow rate was 50.5 kg/s and 15.5 kg/s of air was fed into the circumferential cavity along with the 2 kg/s of fuel. With a mass flow rate of 2 kg/s of fuel and 15.5 kg/s of air, an equivalence ratio of 2 would be achieved in the circumferential cavity. To simplify the study and reduce the computational time, air was injected into the circumferential cavity at 2200 K, a representative combustion temperature for an equivalence ratio of 2. This simplification eliminated the need for combustion modeling at this stage of the analysis. To maintain the correct total mass flow rate into the circumferential cavity, the mass flow

TABLE 2: Air inlet port variations

	20-vane		30-vane	
Inlet Name	**Port Diameter**	**Total Inlet Area**	**Port Diameter**	**Total Inlet Area**
Baseline	0.54 cm	3.19 cm^2	0.54 cm	2.40 cm^2
2x	1.08 cm	12.87 cm^2	0.99 cm	8.05 cm^2
3x	1.62 cm	28.75 cm^2	N/A	N/A
Upper Wall	N/A	57.29 cm^2	N/A	37.89 cm^2

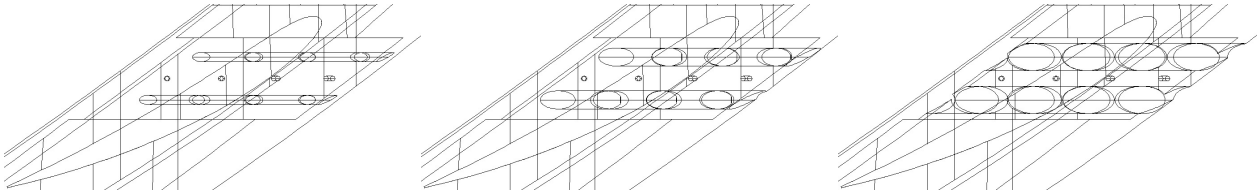

(a) Baseline - ⌀= 0.54 cm (b) 2x - ⌀= 1.08 cm (c) 3x - ⌀= 1.62 cm

FIGURE 6: 20-vane (hybrid vane style) air inlet port variations

rate of the fuel was added to the mass flow rate of air. Using this simplification, 17.5 kg/s of air was injected into the circumferential cavity through the air inlet ports and any density differences or energy lost to vaporize the incoming fuel was neglected. To ensure that all configurations of the computational domains maintained the same total mass flow rates for the full annulus, the total mass flow rate was divided by the corresponding number of vanes since each domain contained only a single vane.

In addition to the engine representative conditions, conditions that could be run in an atmospheric pressure laboratory test rig were also tested using the 20- and 30-vane domains. The rig conditions were scaled to be representative of the engine conditions but operating at standard atmospheric pressure. Table 3 shows the various input parameters for both the engine condition and the rig condition. For all test cases the inlet Mach number remained constant at approximately 0.18 for the engine condition and 0.2 for the rig condition. This Mach number through the combustion section is faster than a conventional engine which slows the incoming fluid to maintain stable combustion. The reduced core flow velocity is not required in a UCC since combustion occurs around the OD of the engine, independent of the core flow. The Reynolds number (Re) at the entrance of the vane passage for the 20-vane domain was approximately 72,000 for the rig condition and 2,250,000 for the engine condition using the initial vane height of 2.2 cm as the reference length. The Re at the exit of the vane passage for the 20-vane domain ranged between 81,100 and 87,300 for the rig condition and 2,830,000 and 2,890,000 for the engine condition. The Re at the entrance to the vane passage of the 30-vane domain was approximately 89,000 for the rig condition and 3,000,000 for the engine condition. At the exit of the vane passage in the 30-vane domain the Re ranged from 118,000 to 129,000 for the rig condition and 3,600,000 to 4,000,000 for the engine condition. The variation in Re at the exit of the vane passage was dependent on the tangential velocity in the circumferential cavity.

In preliminary tests conducted by Bohan [10], it was found that variations in the number of vanes below the circumferential cavity, the shape of the vane below the cavity, the dimensions of the cavity, and variations in the core mass flow rate all had an insignificant impact on the fluid properties within the circumferential cavity. For this reason the air inlet variations, which had a significant effect on the fluid properties in the circumferential cavity, are the focus of this paper. This series of tests was conducted to characterize the flow properties in the circumferential cavity based

TABLE 3: Operating parameters for engine condition and rig condition for complete annulus

Parameter	**Engine Condition**	**Rig Condition**
Operating Pressure	4,000,000 Pa	101,325 Pa
Core Mass Flow Rate	50.5 kg/s	1.466 kg/s
Core Flow Inlet Angle	54°	54°
Core Flow Temp	960 K	530 K
Core Flow Tu	5 %	5 %
Cavity Inlet Mass Flow	17.5 kg/s	0.58 kg/s
Cavity Inlet Flow Temp	2200 K	1000 K
Cavity Inlet Tu	2 %	2 %

on variations in the input flow rates as well as variations in the UCC test section geometry. All four air inlet variations were tested at the cavity inlet mass flow rates shown in Table 3 as well as 75%, 50%, and 25% of these value for the engine condition. The rig condition was only tested at the values shown in Table 3. The values in Table 3 represent the most demanding flight condition. The mass flow rate variation tests simulated throttled conditions while testing the benefits and drawbacks of having more or less vanes below the circumferential cavity.

For each test case, the area-weighted average of tangential velocity, velocity magnitude and density in the circumferential cavity were recorded. The difference between the tangential velocity and the velocity magnitude allowed the flow angle to be calculated. The density was combined with the tangential velocity of the fluid and the known cross-sectional area of the cavity to calculate the mass flow rate in the circumferential cavity. Additionally, the area-weighted averaged total temperature was recorded for the exit face of the domain and plots of the circumferentially averaged total temperatures on the exit plane were created.

RESULTS & DISCUSSION

The preliminary tests conducted by Bohan [10], which all used the baseline air inlet and mass flow rates shown in Table 3, all achieved tangential velocities on the order of 600 m/s for the engine condition and 390 m/s for the rig condition. Applying Eq. 2 to solve for the g-loading on the fluid resulted in values well above 90,000 g's for the engine condition and 40,000 g's for the rig condition. From Figure 2 it can be seen that at an equivalence ratio of 2, any g-loading value above 3,500 g's will result in blowout. Even if a reduced equivalence ratio was used, the g-loading cutoff for blowout is approximately 7,500 g's. Reductions in the mass flow rate into the circumferential cavity did help to reduce the tangential velocity, however, the 100% mass flow rate test cases represent takeoff conditions and other full throttle maneuvers. The engine must be able to operate at the full range of mass flow rates meaning that simply reducing the mass flow rate into the cavity is not an option to limit the g-load. The g-loadings found in the preliminary study would quickly result in a blowout and an unusable engine as the throttle setting was increased. The tangential velocity of the fluid in the cavity must be reduced to maintain the g-load at an acceptable range at the takeoff condition. The target operational g-loading was 3,500 g's. Under the operation conditions outlined in Table 3, this value represents the maximum loading limit prior to blowout, but based on the findings of Lewis [4], this value also represents the highest flame speeds and thus the maximum benefit from g-load combustion.

Since variations in the cavity dimensions, number or geometry of the vanes, and core mass flow rates did not cause any appreciable reduction in tangential velocity, another alternative was sought to reduce the g-load. Reduction of the injection velocity was investigated by changing the cavity air inlet area. Using the 20- and 30-vane domains, the diameter of the air injection ports were enlarged as discussed previously. For constant mass flow rates, as the inlet area increased the injection velocity decreased. As shown in Table 4 for the 100% cavity inlet mass flow rate for engine and rig conditions, the tangential velocity within the cavity was significantly dependent on the cavity inlet velocity. Figure 7 shows that this dependence is linear. This figure also reveals that this dependence was maintained at lower cavity inlet mass flow rates. Figure 8 shows a seemingly identical result for the 30-vane test cases. Figure 9 shows the resulting relationship between the inlet area and the tangential velocity. This plot is applicable to both the 20- and 30-vane test domains.

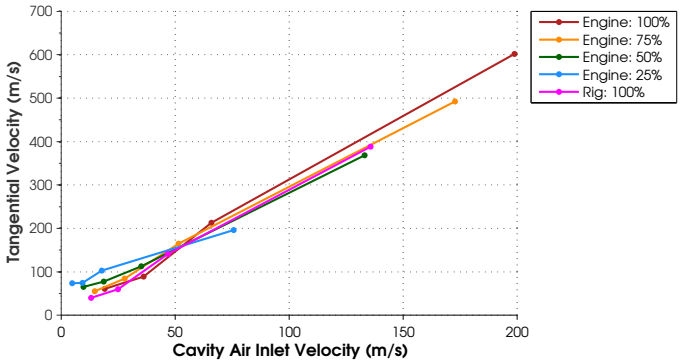

FIGURE 7: Plot of tangential velocity vs. cavity air inlet velocity for 20 vane engine

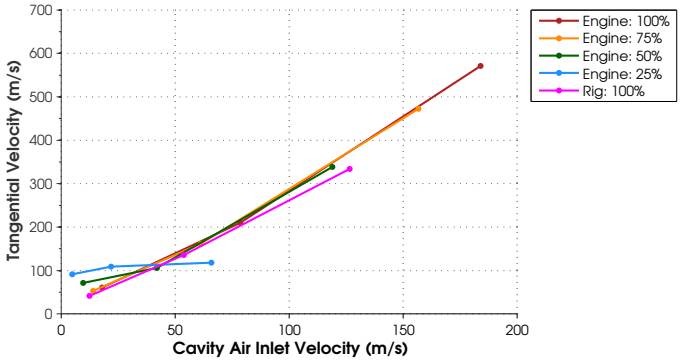

FIGURE 8: Plot of tangential velocity vs. cavity air inlet velocity for 30 vane engine

The mass flow rate in the circumferential cavity was an indicator of how far the fluid travels from the injection hole

TABLE 4: Results for air inlet area variations, 100% cavity inlet mass flow rate, 20- and 30-vane domains

Operating Condition	Inlet Name	Inlet Area[1]	Inlet Velocity	Tangential Velocity	Mass Flow Rate[2]	Pattern Factor	g-Load
20 Engine	Baseline	3.19 cm^2	199 m/s	602 m/s	11.76 kg/s	0.79	97,000
20 Engine	2x	12.87 cm^2	66 m/s	213 m/s	3.79 kg/s	0.41	12,100
20 Engine	3x	28.75 cm^2	36 m/s	89 m/s	1.67 kg/s	0.35	2,100
20 Engine	Top Wall	57.29 cm^2	19 m/s	61 m/s	1.20 kg/s	0.34	1,000
20 Rig	Baseline	3.19 cm^2	136 m/s	388 m/s	0.36 kg/s	1.66	40,300
20 Rig	2x	12.87 cm^2	47 m/s	141 m/s	0.12 kg/s	0.37	5,300
20 Rig	3x	28.75 cm^2	25 m/s	60 m/s	0.05 kg/s	0.55	1,000
20 Rig	Top Wall	57.29 cm^2	13 m/s	40 m/s	0.04 kg/s	0.64	400
30 Engine	Baseline	2.40 cm^2	184 m/s	571 m/s	10.98 kg/s	0.21	87,000
30 Engine	2x	8.05 cm^2	79 m/s	210 m/s	4.08 kg/s	0.43	11,800
30 Engine	Top Wall	37.89 cm^2	18 m/s	67 m/s	1.15 kg/s	0.32	1,200
30 Rig	Baseline	2.40 cm^2	127 m/s	334 m/s	0.44 kg/s	0.22	30,000
30 Rig	2x	8.05 cm^2	54 m/s	136 m/s	0.13 kg/s	0.19	5,000
30 Rig	Top Wall	37.89 cm^2	12 m/s	41 m/s	0.04 kg/s	0.23	450

[1] Total inlet area for the domain section
[2] Cross-sectional mass flow rate through circumferential cavity

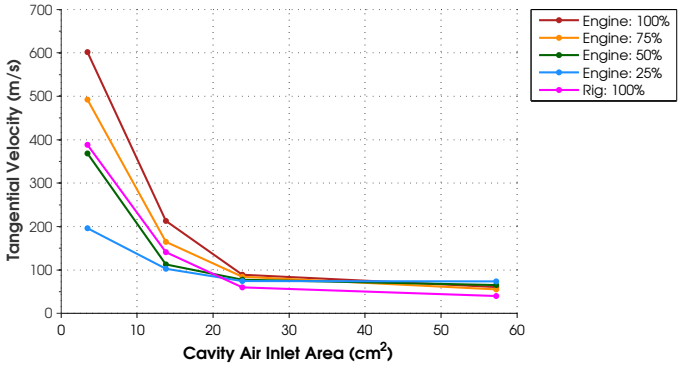

FIGURE 9: Plot of tangential velocity vs. cavity air inlet area

to its exit into the core flow. Since the fluid does not enter the cavity and immediately exit, there was a build up of fluid. The amount of fluid transported in the cavity was proportional to the number of inlets upstream of a reference location whose fluid has not exited the cavity. Larger mass flow rates mean that fluid was staying in the cavity longer and thus traveling farther before exiting. Dividing the cavity mass flow rate from Table 4 by the inlet mass flow rate per vane section (Total cavity inlet $\dot{m}$/vane count), the number of vanes and the physical distance between the inlet and exit position were determined. These measurements were verified by interrogating the streamlines in the CFD solutions. Figure 10 shows the streamlines in the circumferential cavity for the 20-vane domain at engine conditions for the baseline and 3x air inlets. Using the tangential velocity from Table 4 and the arc length traveled, the residence time was computed. The resulting residence times varied between 0.0024 - 0.0027s for the 20-vane engine conditions and 0.0034 - 0.0038s for the rig condition. The 30-vane domain had the same residence time for the engine condition (0.0026 s), but a slightly longer residence time for the rig condition at 0.0039 - 0.0043s.

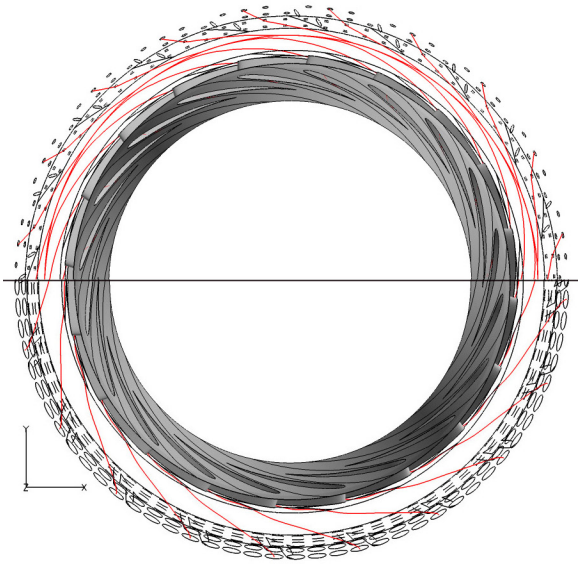

FIGURE 10: Streamlines in the circumferential cavity as viewed from upstream (baseline inlet above, 3x inlet below)

In Figures 7 and 8 it can be seen that the lower cavity mass flow rates (50% and 25%) operating with the larger diameter inlets (slower velocity inlets) achieved faster cavity tangential velocities than the higher mass flow rate cases using the same inlets. This anomaly was the result of the lower mass flow rates entraining core flow fluid into the cavity. Another effect of the entrained core flow in the circumferential cavity was a greatly reduced cavity temperature. The flow pattern in the cavity for the lower mass flow rates revealed a bulk flow in the circumferential direction in conjunction with a swirl component. This pattern was not observed in the higher flow rate cases which only had a circumferential flow component.

In Figures 7, 8 and 9 it can be seen that the rig condition tangential velocity results were closely matched to the 50% mass flow rate engine condition despite a large difference in operating pressure, mass flow rate and inlet temperature. The results are similar because the resultant inlet velocities were very closely matched confirming that the inlet velocity is the driving parameter in controlling tangential velocity regardless of the remaining parameters.

The combustor section exit temperature profile is of critical importance to the turbine blade durability. The temperature profile, or pattern factor (PF), establishes the work potential of the turbine rotor along with setting the cooling flow requirements to the airfoil. The PF as defined by Mattingly et al. [1] is shown in Eq. 4. All station 4 temperatures in this equation were taken as total temperatures on the exit plane. The PF for each 100% cavity inlet mass flow rate test case was shown previously in Table 4. For comparison purposes, the PF of a traditional combustor system is 0.20.

$$PF = \frac{T_{t4max} - T_{t4avg}}{T_{t4avg} - T_{t3}} \tag{4}$$

Ideally, the temperature in the middle third of the blade would be the hottest with the temperature decreasing toward the endwalls. Because endwalls are difficult to cool and there are other complications with hot gas ingestion in the seams between components along the ID endwall and over the blade tip in an actual engine , it is important to keep these surfaces as cool as possible. The exit temperature profile was impacted by the variation of the air inlet area. Figure 11 shows the circumferentially averaged total temperatures for each cavity inlet diameter variation using 100% cavity inlet mass flow rate for the 20-vane domain. Figure 12 shows the same results for the 30-vane domain. In all cases the OD endwall temperature remained fairly constant. The ID endwall, however, was the region most impacted by the air inlet diameter variation, specifically for the 20-vane domain. With the 20-vane domain, higher inlet velocities resulted in higher ID endwall temperatures. There was not a direct linear relationship that applied to the results since the 3x diameter case resulted in a lower ID endwall temperature than the top wall injection case. This relationship does show, however, that slower tangential velocities do not allow the fluid exiting the circumferential cavity to completely penetrate the core flow and heat the endwall as it is convected downstream. The rig condition exit temperature profiles for each inlet area variation followed a similar pattern as the 20-vane engine condition. Again, the larger inlet areas had the lowest temperatures at the endwalls and a relatively uniform maximum temperature across the middle of the passage span.

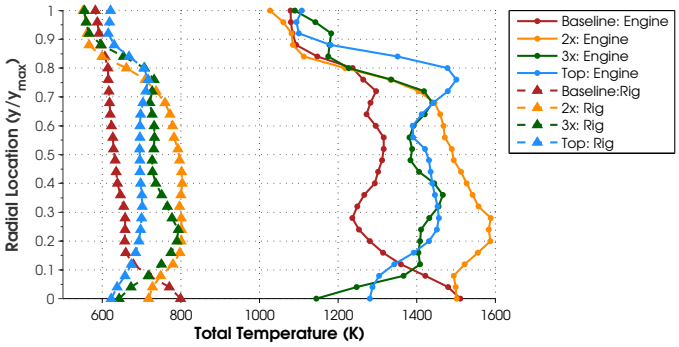

FIGURE 11: Circumferentially averaged total temperatures for inlet diameter variations using 100% cavity inlet mass flow rate, 20-vane domain

In general the 30-vane domain produced more uniform results across the entire vane passage than the 20-vane domain for all inlet diameters tested.

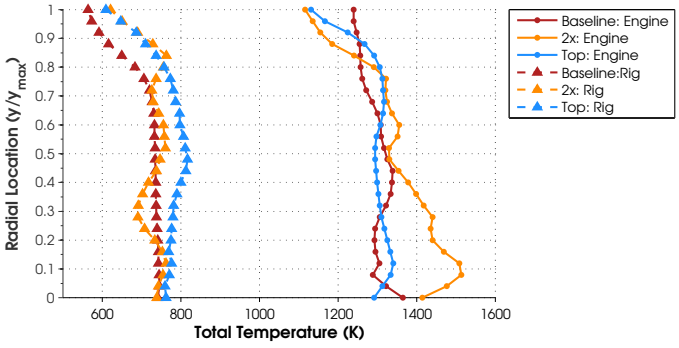

FIGURE 12: Circumferentially averaged total temperatures for inlet diameter variations using 100% cavity inlet mass flow rate, 30-vane domain

To understand why the exit temperature changes with varying inlet diameters, contour plots of the total tempera-

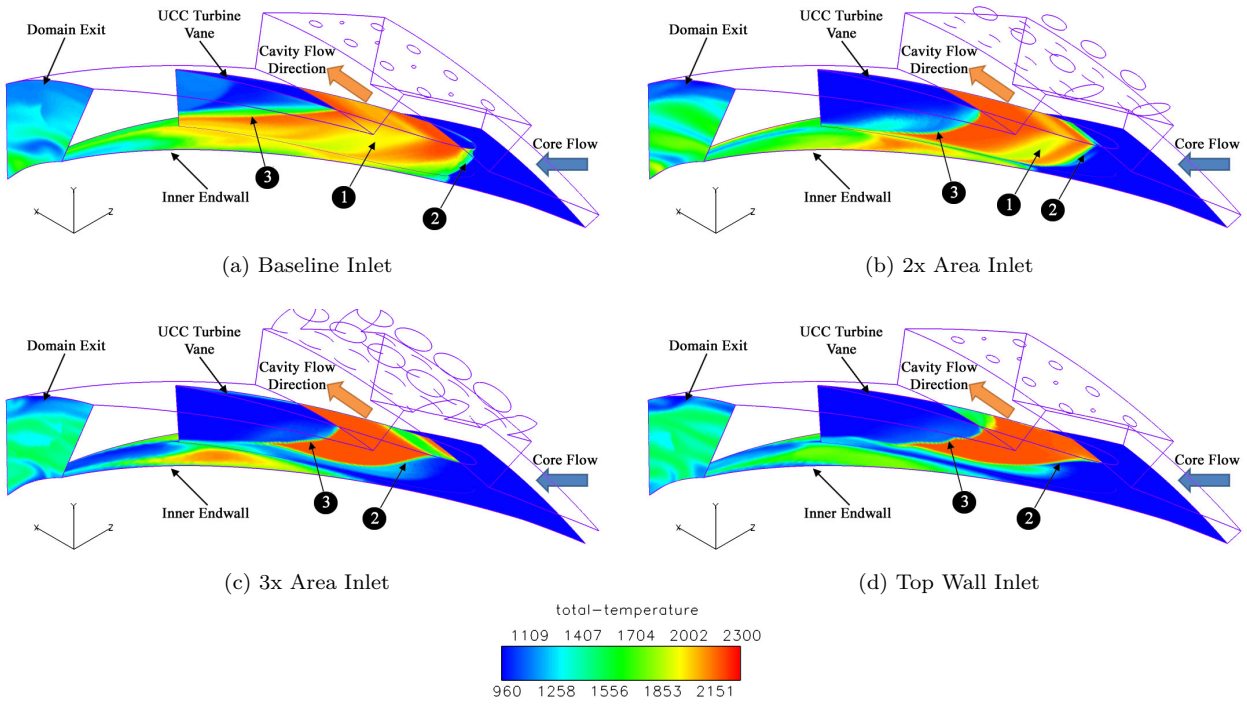

(a) Baseline Inlet

(b) 2x Area Inlet

(c) 3x Area Inlet

(d) Top Wall Inlet

(e) Legend

FIGURE 13: Total temperature contours on engine components using 100% cavity inlet mass flow, 20-hybrid vane domain under engine conditions

ture on the vane, ID endwall and domain exit are shown in Figure 13 for the 20-vane domain operating at 100% cavity inlet mass flow rate for each cavity inlet port size variation. These figures also show the variation of temperature on the domain exit plane in the circumferential direction. In the baseline and 2x diameter inlet test cases, region 1 highlights the areas on the suction surface that were cooled by OD core flow that was entrained by the high velocity cavity flow and swirled into the vane. The profile of the hot fluid on the vane surface after exiting the cavity was directly proportional to the velocity of the fluid in the circumferential cavity. Faster cavity flows had little or no curvature at location 2, but due to the momentum of the fluid exiting the cavity, the profile at location 3 was almost linear. The 3x and top wall inlet domains showed more curvature at location 2, to the extent that the flow on the vane surface did not reach the endwall. There was still flow downstream, however, that swirled off the vane surface and caused ID endwall heating. Additionally, the flow at location 3 did not have the same linear profile observed in the baseline case resulting in a reduced heated footprint. A smaller heated area on the vane surface means that there will be less area to cool in future iterations of the analysis. Because the endwall surface is difficult to cool and ingestion of hot gases into the ID engine seals could result in catastrophic failure, the ideal situation is to have no excess heating of either endwall.

CONCLUSION & FUTURE WORK

The dominant factor controlling the velocity in the circumferential cavity was the inlet velocity of the air feeding the cavity. Larger inlet velocities resulted in larger cavity velocities and vise versa. The cavity inlet velocity was directly related to the area of the inlet, the mass flow rate of fluid into the cavity and the temperature of the incoming air. The residence time remained relatively constant for all inlet geometries varying between 0.0024 and 0.0027 seconds for the engine condition. The number of turbine vanes located below the circumferential cavity did have a minimal effect on the tangential velocity in the cavity. The primary cause of this variation, however, was not due to the number of vanes but rather an overall difference in inlet area resulting from differences in the number of inlets in the complete array. The largest impact resulting from variations in the number of vanes was on the exit temperature profiles. The spacing of the vanes modified the fluid flow pattern between the vanes with a more uniform temperature distribution obtained at the domain exit from the larger vane count.

It was shown that the 3x air inlet diameter in the 20-

vane domain provided the results closest to the target g-load and the most desirable exit temperature profile. Since the maximum benefit for g-loaded combustion occurs at 3,500 g's, the cavity inlet diameter could be modified slightly to adjust the tangential velocity to a maximum value of 114 m/s. The exit temperature profile for the 3x case resulted in the coolest temperatures at the endwalls and the hottest temperatures fairly uniformly distributed across the middle of the passage. The area of the heated portion of the suction surface of the vane for this case also showed a reduced heated footprint which will require less cooling in future iterations of the vane.

The next steps in the fighter-scale UCC analysis includes incorporating reacting flow models to simulate combustion rather than bringing air into the cavity at combustion temperatures. Further analysis will investigate creating a common inlet to ensure a balanced pressure distribution through the UCC.

REFERENCES

[1] Mattingly, J. D., Heiser, W. H., and Daley, D. H., 1987. *Aircraft Engine Design*. AIAA, Washington D.C.

[2] Zelina, J., Sturgess, G. J., and Shouse, D. T., 2004. "The Behavior of an Ultra-Compact Combustor (UCC) Based on Centrifugally-Enhanced Turbulent Burning Rates". *AIAA Paper No. 2004-3541*.

[3] Zelina, J., Shouse, D. T., and Hancock, R. D., 2004. "Ultra-Compact Combustors for Advanced Gas Turbine Engines". *Proceedings of ASME Turbo Expo '04*, June. 2004-GT-53155.

[4] Lewis, G. D., 1973. "Swirling Flow Combustion - Fundamentals and Application". *Presented at AIAA/SAE 9th Propulsion Conference, Las Vegas, Nevada*, November. AIAA Paper No. 73-1250.

[5] Sirignano, W. A., Delplanque, J. P., and Liu, F., 1997. "Selected Challenges in Jet and Rocket Engine Combustion Research". *33rd AIAA/ASME/SAE/ASEE Joint Propulsion Conference, Seattle, WA*. AIAA-97-2701.

[6] Langston, L. S., 1980. "Crossflows in a Turbine Cascade Passage". *Journal of Engineering for Power,* ***102***, pp. 866 – 874.

[7] Hermanson, K. S., and Thole, K. A., 2000. "Effects of Mach Number on Secondary Flow Characteristics". *Journal of Turbo and Jet Engines,* ***17***, pp. 179 – 196.

[8] Hermanson, K. S., and Thole, K. A., 2000. "Effects of Inlet Conditions on Endwall Secondary Flows". *Journal of Propulsion and Power,* ***16***(2), March-April, pp. 286 – 296.

[9] Baskharone, E., 2006. *Principles of Turbomachinery in Air-Breathing Engines*, first ed. Cambridge University Press, New York.

[10] Bohan, B., 2011. "Analysis of Flow Migration in an Ultra-Compact Combustor". Master's thesis, Air Force Institute of Technology, WPAFB, OH. AFIT/GAE/ENY/11-M02.